Canopy structure effects on the wind at a complex forested site

Boudreault, Louis-Etienne; Bechmann, Andreas; Sørensen, Niels N.; Sogachev, Andrey; Dellwik, Ebba

Published in:
Journal of Physics: Conference Series (Online)

Link to article, DOI:
10.1088/1742-6596/524/1/012112

Publication date:
2014

Document Version
Publisher's PDF, also known as Version of record

Canopy structure effects on the wind at a complex forested site

2014 J. Phys.: Conf. Ser. 524 012112

(http://iopscience.iop.org/1742-6596/524/1/012112)

Canopy structure effects on the wind at a complex forested site

L.-É. Boudreault, A. Bechmann, N.N. Sørensen, A. Sogachev, and E. Dellwik
DTU Wind Energy, Frederiksborgvej 399, DK-4000 Roskilde, Denmark.
E-mail: lbou@dtu.dk

Abstract. We investigated the effect of the canopy description in a Reynolds-averaged Navier-Stokes method based on key flow results from a complex forested site. The canopy structure in RANS is represented trough the frontal area of canopy elements per unit volume, a variable required as input in canopy models. Previously difficult to estimate, this variable can now be easily recovered using aerial LiDAR scans. In this study, three approaches were tested which were all based on a novel method to extract the forest properties from the scans. A first approach used the fully spatial varying frontal area density. In a second approach, the vertical frontal area density variations were ignored, but the horizontally varying forest heights were kept represented. The third approach ignored any variations: the frontal area density was defined as a constant up to a fixed tree height over the whole domain. The results showed significant differences among the cases. The large-scale horizontal heterogeneities produced the largest effect on the variability of wind fields. Close to the surface, specifying more details about the canopy resulted in an increase of $x-y$ area-averaged fields of velocity and turbulent kinetic energy.

1. Introduction

The wind speed, turbulent and scalar fluxes are modified by the heterogeneities present in forests [1, 2]. The more clearings, forest edges and density variations a canopy contains, the more likely the flow within and above the canopy will be subject to gradients and develop differently. The local wind field could thus be significantly modified by these heterogeneities. Predicting the wind field using numerical simulations in those circumstances becomes a technically difficult task and can have consequences for different applications and several areas of research. For example, the installation of wind turbines in and close to forests is becoming a more common practice within the wind energy industry due to a decrease in high quality sites availability. In the RANS simulations by [3], it is reported that the wind field is sensitive to the canopy density and that the latter contributes in great part to the simulation uncertainty. It is also mentioned that the simulation results are strongly dependent on the wind direction. In [4], the high turbulence intensity zones over a fragmented forest landscape were pointed out as the cause of wind damage occurrences on trees. Physically, the creation of near-surface wind gusts generated by the local heterogeneities was mentioned as the source of these damaging occurrences. In fire propagation modeling, a study [5] pointed out that the density of the forest cover was related to the fire intensity and that the wind spatial variability increased for larger clumps of heterogeneities [*see also*, 6]. The canopy structure description in this context is thus becoming an important issue.

An approach often employed to model the effect of the canopy in numerical modeling is the

distributed drag formulation, using a momentum sink S_d as:

$$S_d = -C_d a|u|u_i, \tag{1}$$

where C_d is the drag coefficient, u_i the mean wind velocity components in the i direction and $|u|$ denotes the velocity magnitude. The specification of the canopy structure is performed using the variable a — the frontal area density. This variable is defined as the area of leafs, branches and stems opposing the wind flow [m^2] per unit volume [m^3]. Another important variable of consideration is the tree height h_{max}, which indicates the level below which the drag terms should be applied. However, wind modelers are often constrained by limited input information. Simplifications in the specification of a and h_{max} are therefore often necessary. To verify if such simplifications would be justified, we investigated the differences produced in the wind field by canopy descriptions of varying complexity. A series of tests were performed using a CFD model, in which the canopy description was successively degraded. A sensitivity analysis of the wind direction using a fully detailed canopy was also performed.

2. Methodology

2.1. Test site description

The Skogaryd site is a forested site dominated by Norway spruce located $\simeq$ 50 km from the west coast of Sweden. A 38-m-tall mast located at 58°21′50.5”N, 12°8′59.4”E, was the basis for the experiment and was equipped with six sonic anemometers (Metek USA-1 Basic), which were mounted at 1.2, 6.5, 12.5, 18.5, 31.0 and 38.4 m above the local ground level. During the experiment, aerial LiDAR scans of the forest surrounding the tower were performed. A complete description of the experimental method can be found in [7]. The terrain was fairly flat in the domain as the difference between the highest and the lowest elevation point was 35 m.

2.2. CFD model

The CFD model was based on the RANS equations using the standard $k-\epsilon$ model [8]. For wind power production, the high wind speed situations are the most relevant. They generally coincide with neutral stratification which motivated the focus on the neutral case only. For the near-surface flow in these situations, the influence from the Coriolis force is small, except deep inside the canopy, and it was therefore neglected. The terrain elevation was assumed flat in the simulations. The source term in eq. 1 and an additional source term in the transport equation of dissipation ϵ were added in the model to account for the effect of the canopy [9, 10]. The turbulence model constants were set to $C_\mu = 0.06$, $\kappa = 0.4$, $\sigma_k = 1.0$, $\sigma_\epsilon = 2.1$, $C_{\epsilon 1} = 1.52$ and $C_{\epsilon 2} = 1.83$. A polar grid of 30 km diameter surrounding an inner 4×4 km^2 Cartesian grid was used. The computational grid had an $x-y$ resolution of 10 m in the inner region. A hyperbolic mesh generator [11] was used to make a three-dimensional volume grid. The domain height was set to 4 km with a vertical near-ground resolution of 0.03 m, from where it was expanded to a resolution of about 1 m at a 30 m height above the ground. Simulation tests indicated that the numerical solution was grid-independent. Inside the inner domain, where the forest information was available, a roughness height of $z_0 = 0.03$ m was prescribed at the ground boundary below the canopy. Outside this domain, tests showed that a roughness of $z_0 = 0.03$ m was appropriate to reproduce the farfield conditions. The set of equations were solved using the EllipSys3D flow solver [12–14]. The Leonard's third-order accurate QUICK scheme [15] was used on the advective operators and the standard second-order central difference scheme for all remaining terms was used. As boundary conditions, values of u, k and ϵ in accordance with log-law relationships were prescribed at the inlet and at the top of the domain. Standard Neumann conditions (zero normal gradients) were used at the outlet. The inlet boundary condition extended over a 270° portion on the exterior boundary of the polar domain and the outlet boundary condition extended over a

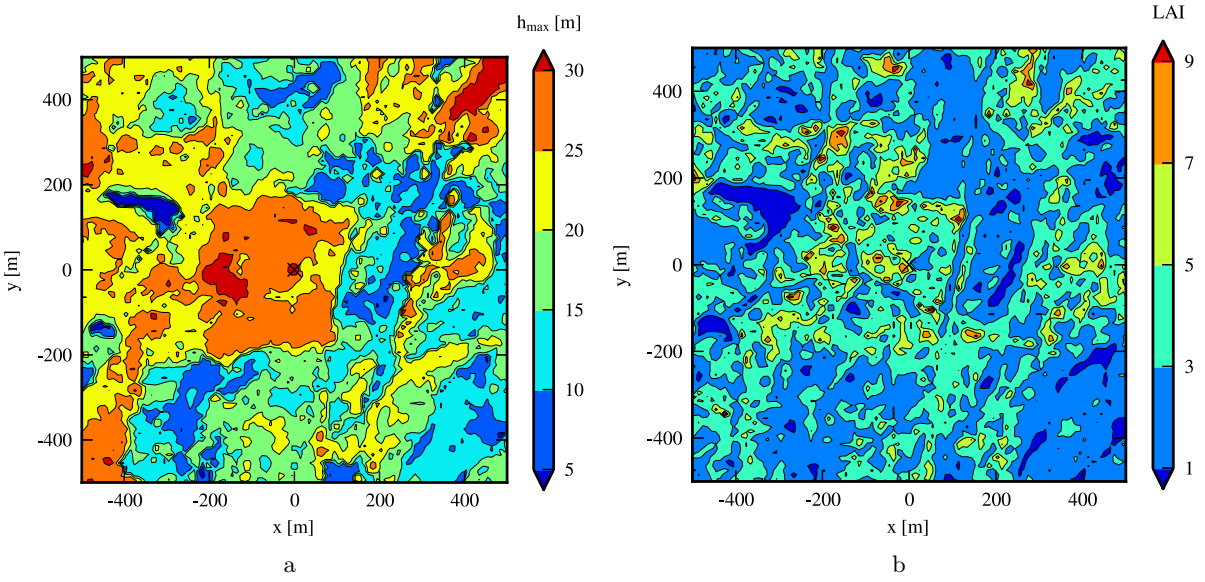

Figure 1. (a) Tree height and (b) leaf area index, as obtained from the method described in *Case 1*.

90° portion. Standard log-law wall functions were applied at the ground boundary, as described in [14]. The wind direction simulated for the main results is 270° (westerly wind).

2.3. Case study

In the following tests, three different cases including different levels of canopy structure complexity were used. These cases were defined based on possible input information at the disposal of developers. In the first case, denoted *Case 1*, varying profiles of a in x, y and z as well as varying forest heights were used. This setup was the reference case from which the wind results obtained from the other two less detailed cases were compared. In *Case 2*, the frontal area density was kept constant with height but the forest height was spatially variable. In *Case 3*, a constant forest height and a constant frontal area density a was imposed throughout the domain. For all cases, the canopy information was prescribed inside and near the inner area of the CFD grid over 5×5 km^2. More specifically, the a and h_{max} distribution for each cases were defined as follows:

Case 1

A complete description of the method used for this case can be found in [7]. In this method, the distribution of a was calculated based on aerial LiDAR scans. Compared to other remote sensing methods, LiDAR scans generally provide the most detailed description as it can reveal the 3D structure of the canopy. The resulting output is a grid of ijk index containing discrete values of a. In this method, the forest grid generated had a bin radius of $r = 10$ m, a grid spacing of $\Delta x = \Delta y = 10$ m and layers of $\Delta z = 1.0$ m thickness. The forest properties obtained can be visualized in Fig. 1 and Fig. 2 where the leaf area index (LAI) was obtained by summing the a^{ij} values over the k index:

$$LAI^{ij} = \sum_{k=1}^{n_h} a_k^{ij} \Delta z \ , \quad \text{where} \quad n_h = ||h^{ij}/\Delta z||. \tag{2}$$

Case 2

The distribution of constant a values was calculated based on the local leaf area index and

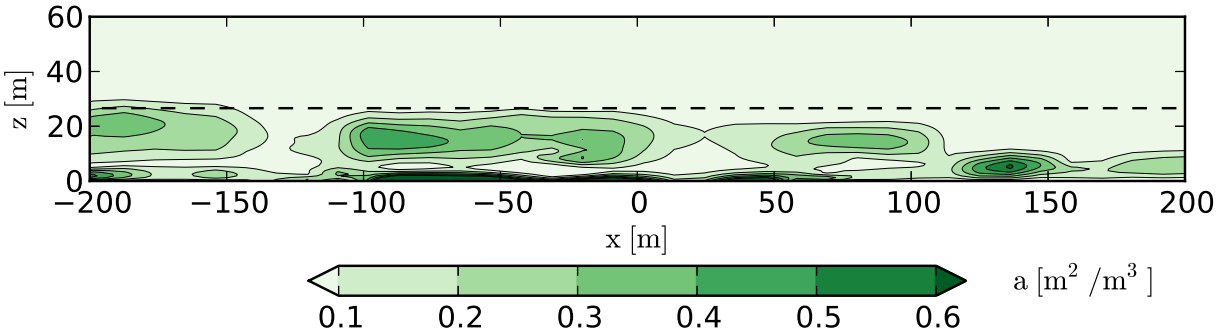

Figure 2. Frontal area density contours as retrieved from aerial LiDAR scans for a transect at $y = 0$ m passing trough the mast location ($x = 0$ m). The dash line indicate the constant forest height fixed in *Case 3* ($h_{max} = 26.6$ m).

h_{max} was obtained from the method in *Case 1*. To do this, the LAI at the ij positions was kept the same as calculated in *Case 1*. The frontal area density at the ijk positions was then fixed to $a^{ijk} = LAI^{ij}/h^{ij} = cst$.

Case 3

To determine a fixed a and h_{max} value for *Case 3*, we considered an averaging area of 200×200 m^2 centered around the mast location $(x, y) = (0, 0)$. This area was chosen as it was fairly homogeneous (Fig. 1), i.e. the trees were of the same species and similar heights. The mean values of $\overline{LAI}$ and $\overline{h}_{max}$ were then calculated based on the estimates calculated from the method in *Case 1*. The values obtained were $\overline{LAI} = 4.5$ and $\overline{h}_{max} = 26.6$ m. The frontal area density was therefore fixed to $a = \overline{LAI}/\overline{h} = 0.169$ m^2/m^3 throughout the domain over a fixed canopy height of $\overline{h} = 26.6$ m (showed as a dashed line in Fig. 2).

3. Results

The simulations for the three cases described in Section 2.3 were compared. The velocity magnitude u and the turbulent kinetic energy tke were used as comparison variables. The profiles obtained from the numerical results in the three cases were first validated with the mast measurements. The focus was put on results of a 1×1 km^2 area centered on the tower location below a height of 50 m above the ground level. This choice was motivated by the fact that an internal boundary layer will grow at the edges of the 5×5 km^2 area where the forest was prescribed. It was evaluated to be about 50 m thick over this area [16]. Area-averaged profiles over 1×1 km^2 areas at different heights were then compared between the cases. In these results, the root-mean-square deviation ($RMSD$) estimator was used and was defined as:

$$RMSD_{\phi_{12}} = \sqrt{\frac{\sum_{i=1}^{n}\sum_{j=1}^{m}(\phi_{1,ij} - \phi_{2,ij})^2}{n \times m}}, \tag{3}$$

as well as the percentage difference (%Diff) estimator,

$$\%\text{Diff}_{\phi_{12}} = \frac{\phi_{2,ij} - \phi_{1,ij}}{\phi_{1,ij}} \times 100, \tag{4}$$

where ϕ_1 and ϕ_2 were field variables under consideration in two different cases (*e.g. Case 1* and *Case 2*).

Table 1. Root-mean-square deviation ($RMSD$) over a 1×1 km^2 area between the reference wind direction (270°) and perturbation values for the *Case 1* setup at 50 m AGL.

Wind direction	$RMSD_{u/u_{50m}}$	$RMSD_{tke/u^2_{50m}}$
$270° - 1°$	0.0069	9.91×10^{-5}
$270° + 1°$	0.0078	9.06×10^{-5}
$270° - 5°$	0.0230	3.26×10^{-4}
$270° + 5°$	0.0260	4.61×10^{-4}
$270° - 10°$	0.0292	7.39×10^{-4}
$270° + 10°$	0.0188	4.18×10^{-4}
$270° - 15°$	0.0299	8.15×10^{-4}
$270° + 15°$	0.0187	4.98×10^{-4}

3.1. Wind direction sensitivity

The high variability of the canopy structure induces different wind fields with different wind directions, as reported in [3]. Therefore, an important aspect to verify first is how sensitive this effect could be. A wind direction analysis around the reference wind direction (270°) was thus performed for angles of ±1°, ±5°, ±10° and ±15°. This test used the full canopy structure description as obtained by the LiDAR measurements (*Case 1*). In Table 1, the $RMSD$ for the wind directions ±1° was small for both u/u_{50m} and tke/u^2_{50m} (≈ 0.0075 and 9.5×10^{-5}, respectively). For wider angles, the $RMSD_{u/u_{50m}}$ remained similar when the wind direction was changed (ranging between 1.8×10^{-2}–2.9×10^{-2}) but the $RMSD_{tke/u^2_{50m}}$ showed a higher sensitivity and variability (ranging between 3.26×10^{-4}–8.15×10^{-4}). The error due the wind direction is thus expected to remain similar for the velocity field within wind sectors of 10–30°; but larger errors and variability are expected in the *tke* field. Below a 2° wide sector, the differences in the flow field were negligible. As the wind direction variability in the present simulations can only be reproduced with spatially varying a and h_{max}, a minimal variability in the wind direction can only be obtained by including a description of the larger clumps of heterogeneities, as they produce the largest effect on the wind field [5].

3.2. Profiles validation

The summed $RMSD_{u/u_{38m}}$ between the mast measurements and the simulation results at each of the instrument level locations were compared (Fig. 3a and 3b). The $RMSD_{u/u_{38m}}$ was the lowest for *Case 1* (*Case 1*: 0.0358; *Case 2*: 0.0366; *Case 3*: 0.0385). The profiles in *Case 1* and *Case 2* compared better to measurements than *Case 3* inside the forest and the profile in *Case 3* was in closer agreement above the canopy (Fig. 3a). A secondary maximum close to the surface was observable in *Case 1* (Fig. 3a), a characteristic that was absent in the other two cases. This characteristic was attributed to specifying a varying distribution of a in the vertical direction above the surface. For the tke/u^2_{38m} (Fig. 3b), the lowest $RMSD_{tke/u^2_{38m}}$ was obtained for *Case 2* (*Case 1*: 0.0926; *Case 2*: 0.0920; *Case 3*: 0.0923). The profiles in *Case 1* and *Case 2* were generally closer to the error range of the measurements than in *Case 3* (Fig. 3b). An overprediction of tke/u^2_{38m} was apparent inside the canopy in *Case 3* (Fig. 3b).

3.3. Fields comparison

In the following results, the upstream farfield velocity at 50 m above the ground level was used to normalize the fields. Visual inspection of the fields of u/u_{50m} for *Case 1* and *Case 2*

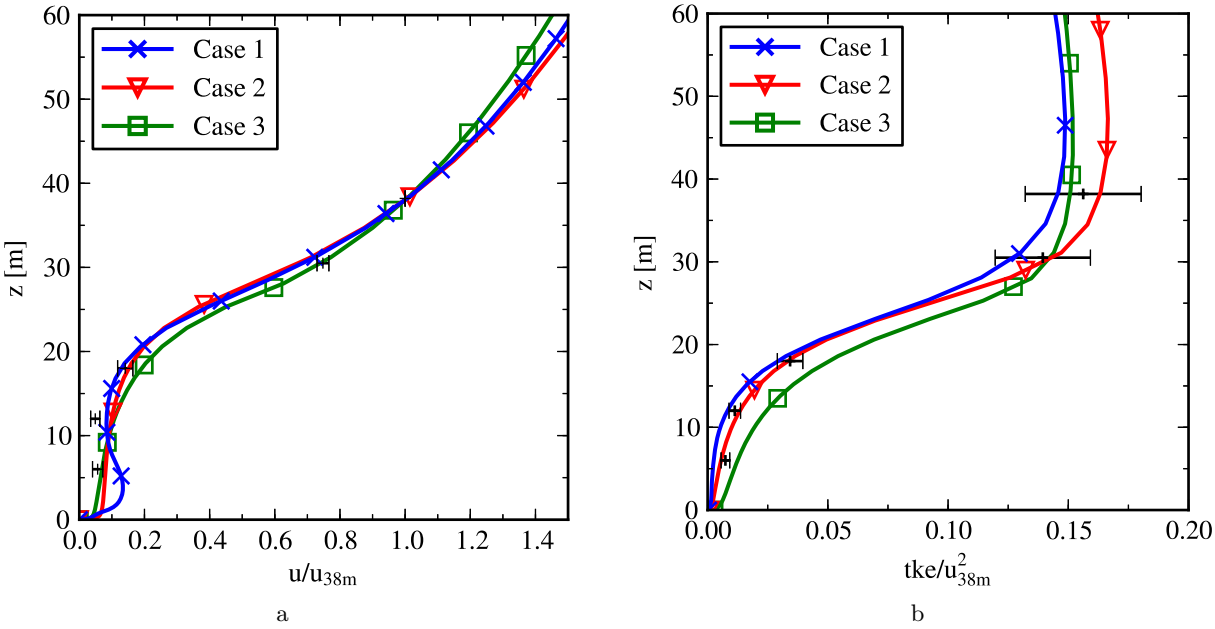

Figure 3. Profiles of (a) u/u_{38m} and (b) tke/u^2_{38m} for all 3 cases compared with mast measurements. The normalization velocity u_{38m} was taken at the 38 m level at the mast location. The error bars on the measurements shows the extent of 1 standard deviation around the mean value.

showed similarities (Fig. 4a, 4b), as the contour patterns generally coincided, but with different mean values. The mean velocity was higher in *Case 1* ($u/u_{50m} = 0.64$) compared to *Case 2* ($u/u_{50m} = 0.62$) and *Case 3* ($u/u_{50m} = 0.57$). For the tke/u^2_{50m} fields (Fig. 4c, 4d), the average value was comparable for all cases ($tke/u^2_{50m} \approx 0.032$). The tke/u^2_{50m} was different between *Case 1* and *Case 2* above the central high and dense forest patch ($-200 > x > 200$ m and $-200 > y > 200$ m, Fig. 1a, 1b) as the contours levels differed in location and shape.

The *Case 1-Case 2* and *Case 1-Case 3* percentage difference fields (computed from eq. 4) were compared (Fig. 5). For *Case 2* (Fig. 5a), the % difference in velocity with *Case 1* was globally below 6%. The largest differences were observed along the lines at $y = -200$ and $y = 200$ m, physically located along the north and south forest edges of the central tall trees and dense forest patch (Fig. 1a, 1b). For *Case 3* (Fig. 5b), the difference was generally larger than in *Case 2*. The error was the smallest in the central patch around the mast and in areas where the forest was homogeneous and had similar mean values of forest properties imposed (such areas could be seen along $x = -200$ m and at $(x, y) = (-200, 250)$ m in Fig. 1a, 1b). The largest percentage difference in tke/u^2_{50m} for *Case 2* (Fig. 5c) was inside the central forest patch, in the wake of the patch, as well as in the clearings along $y = -450$ m and at $(x, y) = (-400, 200)$ m. For *Case 3* (Fig. 5d), the largest differences were observed in the clearings.

3.4. Area-averaged profiles

In this section, $x - y$ area-averaged results, denoted by angled brackets $\langle\cdot\rangle$, are presented at different heights. The area-averaged profiles (Fig. 6) clearly indicated higher $\langle u\rangle/u_{50m}$ and $\langle tke\rangle/u^2_{50m}$ in the following order: *Case* 1 > *Case* 2 > *Case* 3. The velocity profiles differed and reached a percentage difference of 8.9% between *Case 1-Case 3* and 3.5% between *Case 1-Case 2* at a height of 50 m. The *tke* profiles almost coincided above 40 m AGL (both *Case*

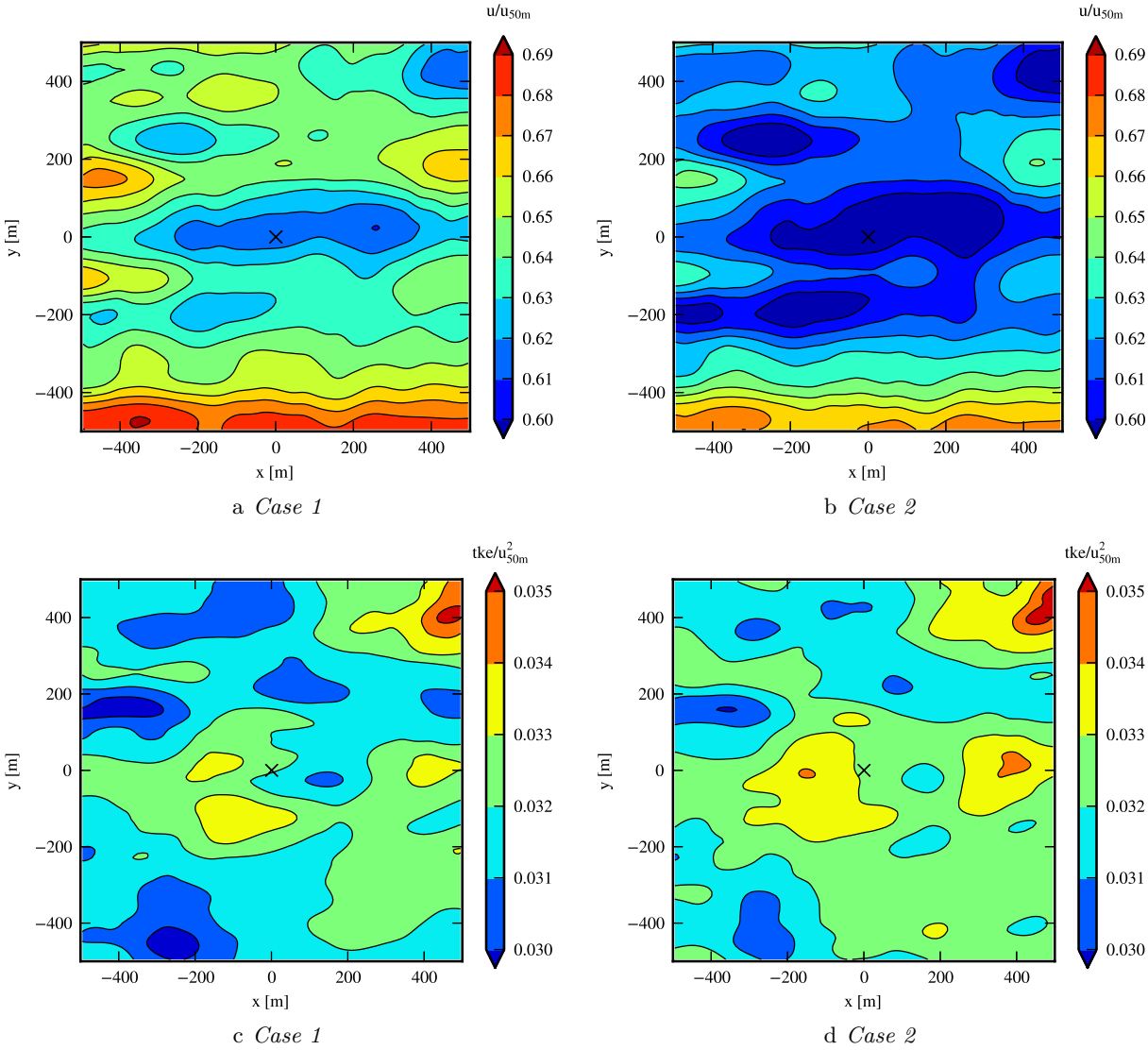

Figure 4. Contours of u/u_{50m} and tke/u_{50m}^2 at a height of 50 m above the ground level for *Case 1* and *Case 2*. The upstream farfield velocity u_{50m} at 50 m was used to normalize the fields. The flow direction goes from left to right.

2 and *Case 3* were below 1.5% of *Case 1* at 50 m AGL). The highest variability (standard deviation) in *Case 1* and *Case 2* were close to the canopy top, *i.e.* around 20 m for the velocity and 15 m for the *tke* profile (no variability was present in *Case 3* as the forest was horizontally homogeneous).

4. Discussion

Several points of discussion could be raised from the results. First, the profiles in Fig. 3 showed that a secondary maximum was produced in *Case 1* while it was absent in the other two cases. This shows that the predicted flow processes within the canopy are different for a method allowing density variations in the vertical direction compared to a method where the profiles are constant. This will affect the predictions in situations where the terrain is complex, *e.g.*

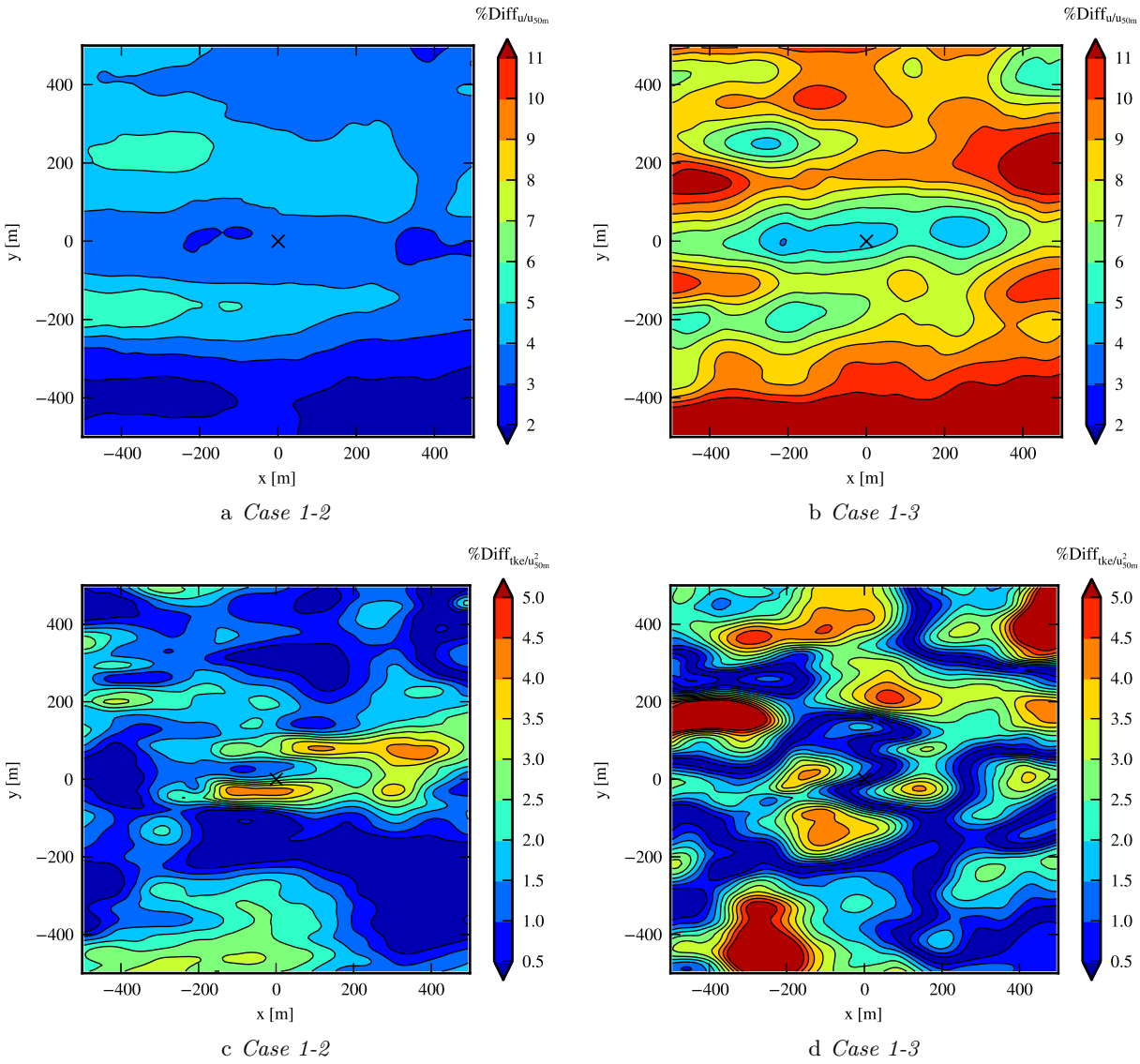

a *Case 1-2* b *Case 1-3*

c *Case 1-2* d *Case 1-3*

Figure 5. Percentage difference in u/u_{50m} and tke/u^2_{50m} between *Case 1* and *Case2* and *Case 1* and *Case 3* at 50 m above the ground level. The upstream farfield velocity u_{50m} at 50 m was used to normalize the fields. The flow direction goes from left to right.

close to forest edges [2] and potentially in steep orography. For the flow above the forest, the velocity profiles were similar but the *tke* profiles showed larger differences. Generally, the profiles agreed well with the measurements since they were close or within the range of one standard deviation of the measurements. However, for the upstream area along $y = 0$ m in the direction in-line with the mast (Fig. 1), the forest was fairly homogeneous which may explain the good comparison, and why only small differences were observed between the profiles. When large heterogeneities were opposing the wind flow, *e.g.* in the central forest patch and over clearings, differences between the methods started to appear (Fig. 5). In Fig. 4, the small variations in canopy density produced small visible differences in the velocity field between *Case 1* and *Case 2*. More significant differences were observed in the turbulence field, even when the forest was homogeneous, as was the case over the central forest patch. The velocity field was thus

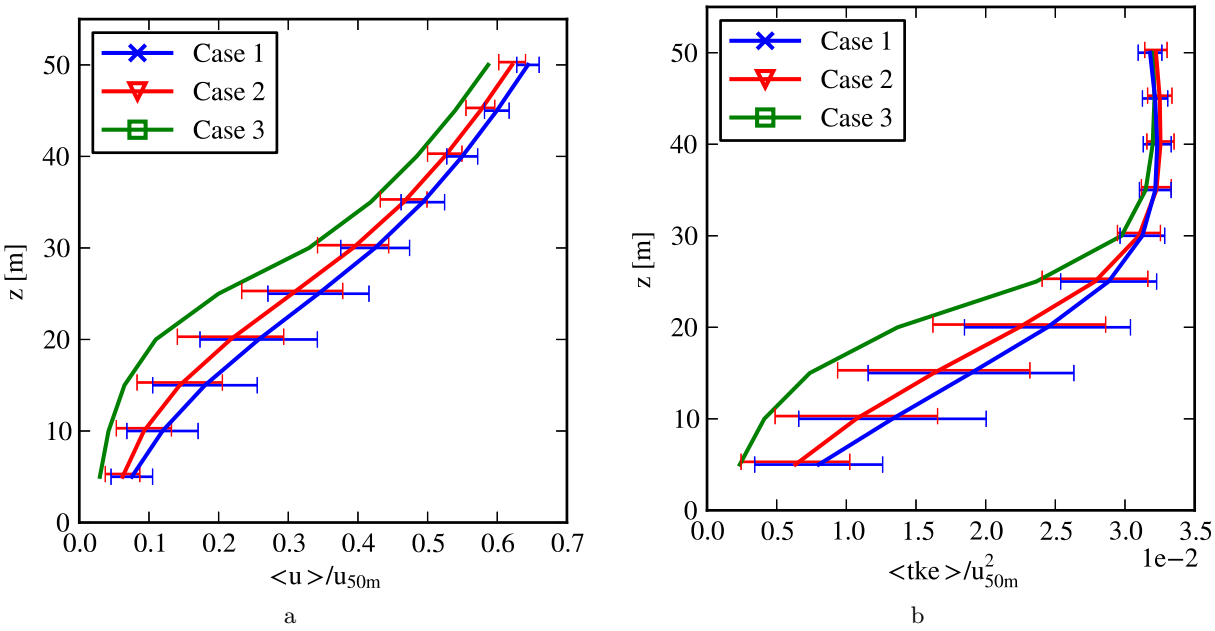

Figure 6. Spatially averaged profiles of (a) $\langle u \rangle / u_{50m}$ and (b) $\langle tke \rangle / u_{50m}^2$ at different heights over the 1×1 km^2 area for all three cases. The upstream farfield velocity u_{50m} at 50 m was used to normalize the profiles. The error bars on the measurements shows the extent of 1 standard deviation around the mean value over the area.

sensitive to changes in larger agglomerations of heterogeneities (*e.g.* along the forest edges of the central forest patch) while the *tke* field showed sensitivity to both the larger and the smaller heterogeneities (Fig. 5). To summarize, the accuracy in the *tke* prediction will be compromised if the smaller scale canopy structures are poorly described. This aspect is however less significant for the velocity field, for which the larger heterogeneities are more important to parameterize.

The area-averaged profiles (Fig. 6) showed that the wind velocity and *tke* increased with an increasing amount of canopy details over the whole investigated height range. The presented results were however based on a simplified case over flat terrain in a 1×1 km^2 area. The effect of the canopy on the wind over a real terrain and a large domain should also be investigated. In complex orography, the flow may interact more strongly with the canopy and alter the wind field accordingly.

5. Conclusion

In this study, RANS simulations involving different levels of canopy structure complexity were performed. Non-negligible differences were found such that:

- the 50 m wind velocity over the 1×1 km^2 showed less sensitivity in wind direction change than the *tke* results;
- the velocity was more sensitive to the larger-scale heterogeneities while the *tke* was more sensitive to the smaller-scale heterogeneities;
- the most detailed methods of canopy structure description produced the highest velocities and *tke* results;
- using methods of the same *LAI* but prescribing a profile of constant vertical density failed to capture the secondary maximum close to the surface.

The results presented here showed that including an increasing amount of smaller heterogeneity variations in the canopy description is important when the site is complex.

Acknowledgements
The authors acknowledge the financial support of the Center for Computational Wind Turbine Aerodynamics and Atmospheric Turbulence sponsored by the Danish Council for Strategic Research, grant number 09-067216, Vattenfall and Vindforsk III, a research program sponsored by the Swedish Energy Agency.

References

[1] Bohrer G, Katul G, Walko R and Avissar R 2009 *Boundary-Layer Meteorology* **132** 351–382
[2] Dellwik E, Bingöl F and Mann J 2013 *Quaterly Journal of the Royal Meteorological Society*
[3] Lopes Da Costa J, Castro F, Palma J and Stuart P 2006 *Journal of Wind Engineering and Industrial Aerodynamics* **94** 603–620
[4] Dupont S and Brunet Y 2006 *Boundary-Layer Meteorology* **120** 133–161
[5] Pimont F, Dupuy J L, Linn R and Dupont S 2011 *Annals of Forest Science* **68** 523–530
[6] Panferov O and Sogachev A 2008 *Agricultural and Forest Meteorology* **148** 1869–1881
[7] Boudreault L E, Bechmann A, Tarvainen L, Klemedtsson L, Shendryk I and Dellwik E *Agricultural and Forest Meteorology.* Manuscript submitted for publication.
[8] Jones W and Launder B 1972 *International Journal of Heat and Mass Transfer* **15** 301 – 314
[9] Sogachev A and Panferov O 2006 *Boundary-Layer Meteorology* **121** 229–266
[10] Sogachev A 2009 *Boundary-Layer Meteorology* **130** 423–435
[11] Sørensen N 1998 Hygrid2D - a 2D mesh generator. Tech. Rep. Technical report Risø-R-827(EN) Risø DTU
[12] Michelsen J 1992 Basis3d - a platform for development of multiblock PDE solvers. Tech. Rep. Technical report AFM 92-05 Technical University of Denmark.
[13] Michelsen J 1994 Block structured multigrid solution of 2D and 3D elliptic PDE's. Tech. Rep. Technical report AFM 94-06 Technical University of Denmark.
[14] Sørensen N 1995 General purpose flow solver applied to flow over hills. Tech. Rep. Risø-R-827(EN), Ph.D. thesis. Risø DTU
[15] Leonard B 1979 *Computational methods in applied mechanical engineering* **19** 59–98
[16] Dellwik E and Jensen N 2000 *Theoretical and Applied Climatology* **66** 173–184